Environmental Science Nano

PAPER

View Article Online
View Journal | View Issue

Cite this: *Environ. Sci.: Nano*, 2019, **6**, 820

Evolution of the reactive surface area of ferrihydrite: time, pH, and temperature dependency of growth by Ostwald ripening†

Tjisse Hiemstra, * Juan C. Mendez and Jiayu Li

Surface area is a crucial property of metal oxides for scaling ion adsorption phenomena. For ferrihydrite (Fh), the value is uncertain. Moreover, it rapidly changes with time, pH, and temperature. In this study, the dynamic change of the reactive surface area has been probed with phosphate for ferrihydrite, produced by ultra-fast neutralization at 20 °C. The initial nanoparticles are very small ($d \sim 1.68$ nm), have a remarkably large specific surface area ($A \sim 1100$ m^2 g^{-1}), and contain on average only 45 Fe atoms. Our data reveal the rapid change of the surface area showing that the rate of growth decreases by nearly three orders of magnitude ($R \sim 0.01$–10 μmol Fe m^{-2} h^{-1}) within one week of ageing. The rate of growth is proportional to the square of the super saturation of the solution $(Q_{so}/K_{so})^2$, which suggests a rate limitation by dual attachment of Fe to a surface site of growth. This process is significantly hindered by the presence of weakly bound organic molecules, particularly at low pH, implying for soils that natural organic matter may considerably contribute to the kinetic stability of the natural iron oxide fraction. Our data also show that the reaction pathways are very different in $NaNO_3$ and NaCl solutions. The decrease of surface area in $NaNO_3$, prepared in traditional batch experiments, can be described excellently with the above rate law implemented in our dynamic model. This model also covers the temperature dependency (4–120 °C) of Fh ageing using an activation energy of $E_a = 68 \pm 4$ kJ mol^{-1}. For traditionally prepared 2LFh, our model suggests that with solely dual Fe attachment, the growth of the primary particles is limited to $d \sim 3$–4 nm ($A \sim 350$–500 m^2 g^{-1}). Larger particles can be formed by oriented attachment of particles, particularly at a high temperature. Using forced hydrolysis at 75 °C, large particles ($d \sim 5.5$ nm) can also be produced directly. According to our model, Ostwald ripening of such 6LFh particles will be limited due to their low solubility.

Received 25th October 2018,
Accepted 29th January 2019

DOI: 10.1039/c8en01198b

rsc.li/es-nano

Environmental significance

Ion adsorption data require scaling to the specific surface area. For ferrihydrite, this crucial property is continuously changing with time due to Ostwald ripening. This change has been traced as a function of pH and temperature covering the time scale of minutes to seven days using phosphate as probe ion. The collected data give insight into the mechanism and rate of growth, *i.e.* dual Fe attachment limited by the size dependent solubility of ferrihydrite. Implemented in a dynamic model, it discloses the ultra-small initial size of Fh particles and predicts the subsequent change of surface area and particle size. It allows a tunable synthesis of this nanomaterial and a suitable scaling of its ion adsorption properties, improving the development of thermodynamic ion adsorption databases.

Introduction

Ferrihydrite (Fh) is a nanoparticle omnipresent in nature and used in environmental engineering. Its properties contribute to the fate of many elements in the geochemical cycle and environmental technology. Ferrihydrite nanoparticles are highly reactive and have a high ion adsorption capacity that is relevant for applications. For this reason, it is used and widely studied as model material to elucidate the adsorption of cations, anions, and organic matter.[1–19] The surface area of ferrihydrite is an essential characteristic particularly from the perspective of surface complexation modelling. One reason is that ferrihydrite particles are usually charged. This charge is scaled to a surface area. It allows calculation of the variable electrostatic energy contribution that largely controls the variation in binding of ions to surfaces in relation to solution

Department of Soil Chemistry, Wageningen University, P.O. Box 47, 6700 AA Wageningen, The Netherlands. E-mail: tjisse.hiemstra@wur.nl; Tel: +31 317 48 2342

† Electronic supplementary information (ESI) available: Flow chamber design, deriving the rate of growth R from the collected data, size-dependency of Stern layer capacitances and adsorption, monolayer density of Fe, polyhedral representation of a non-aged initial Fh particle, influence of initial particle size on ageing, rate limitation by diffusion across the solid–water interface. Ageing of 6LFh. See DOI: 10.1039/c8en01198b

conditions.[7,20–24] In addition, the supposed surface area determines the number of available adsorption sites at a given surface site density. Therefore, proper scaling is crucial for describing ion adsorption behavior of Fh.

Ferrihydrite is easily synthesized in the lab.[25] However, variations in protocols lead to different and not well-known surface areas.[26,27] Moreover, the surface area of ferrihydrite will decrease with time because nanoparticles are thermodynamically unstable and will spontaneously grow. For ferrihydrite, the rate of change depends on controlling factors such as pH, adsorbed ions, and temperature.[28]

Relatively, little information is available about the evolution of the reactive surface area and particle size of Fh immediately after preparing the nanomaterial for use in for instance ion adsorption experiments. Formation of ferrihydrite starts with nucleation and it is followed by the binding of yet unreacted Fe(III), still present in the solution phase. The combination of nucleation and supplementary Fe adsorption results in a polydisperse suspension that initially contains ultra-small nanoparticles with a very high surface area, a high reactivity, and a high instability.

In a Fh suspension, the smallest particles will maintain a labile equilibrium between Fe in solution and the solid phase.[29] Fh particles, larger than a critical size, will spontaneously grow at the expense of the smaller particles that dissolve. This will lead to an increase of the mean particle size. This process of simultaneous growth and dissolution was first described by Ostwald,[30] and therefore, we will refer to this process of coarsening as Ostwald ripening (OR).

For relatively large Fh particles, the rate of growth by classical Ostwald ripening becomes very small, as will be demonstrated in the present study. Nevertheless, experimental data show that Fh particles can still increase significantly in size.[31] This is due to growth by oriented particle attachment.[32] As soon as the Fh particles become sufficiently large, patches of specific crystal faces may develop that allow oriented attachment (OA).[33] Even larger particles may form by fusion as shown for ZnS.[34] Self-assembly of primary Fh particles results in rod-shaped entities as shown with TEM by Murphy *et al.*[35] and more recently, by Burleson and Penn.[31] These units get a typical aspect ratio of 5 ± 1.[31,35] The process of oriented particle attachment typically occurs for Fh particles with a size near ~4 nm and larger.[33] The rate of this particle–particle interaction is second-order-dependent on the suspension concentration of the primary nanoparticles and has a rate constant that depends on the pH and interface structure.[36] The process is most evident during aging at high temperature (60–120 °C) and high pH (10–12).[31]

Ultimately, ferrihydrite transforms into more stable Fe (hydr)oxides. In the presence of dissolved Fe(II), the conversion is accelerated,[37] forming lepidocrocite and goethite within hours. Otherwise, Fh may convert into goethite, hematite, or maghemite.[38–41] This conversion occurs at a relatively large particle size[29] and therefore, it has often been studied at hydrothermal conditions. To quantify the degree of transformation, the difference in rate of dissolution in an oxalate[42–44] or ascorbate solution[45] has been used to assess the amount of Fh left at transformation, or X-ray diffraction and/or EXAFS is used to estimate the amount of crystalline material formed.[41,46,47]

The initial size of primary Fh nanoparticles immediately formed after instantaneous hydrolysis of Fe(III) upon base addition is very small but not well known. It has been proposed that the initial formation of Fh is *via* the formation of ultra-small Fe_{13} nuclei[48] with a Keggin structure having one central tetrahedral Fe. Similar clusters may form in ferritin when loaded with little Fe.[2] Fe_{13} nuclei are stable at very acid conditions but they grow above pH ~ 2 to ferrihydrite.[48] This growth is driven by the adsorption of dissolved Fe-complexes such as dimers.[49,50] Immediately after ultrafast synthesis of Fh at room temperature in a NaCl solution,[51] the particles have a mean particle size of $d \sim 1.8$ nm, a specific surface area of $A \sim 1000\ m^2\ g^{-1}$, and contain $n_{Fe} \sim 60$ Fe.[2]

With classical protocols for Fh synthesis, the specific surface area can be significantly smaller than with fast hydrolysis. Traditionally synthesized two-line ferrihydrite usually has a specific surface area in the range of just $A \sim 530$–$710\ m^2\ g^{-1}$ when kept in the wet state.[27] The corresponding mean particle size is between $d \sim 2.3$–2.9 nm and the number of Fe per particle is $n_{Fe} \sim 140$–325 Fe. When dried, the particles are irreversibly bound together in porous aggregates having a significantly lower reactive surface area.[7,16,52–55]

The above overview illustrates that the particle size and surface area of Fh ultimately used in laboratory experiments may largely differ from the nanoparticles initially formed. At storage, the surface area will further decrease. The present study is meant to quantify the rate of ageing of freshly prepared Fh. We will study the change in reactive surface area of Fh in $NaNO_3$ for a time scale up to one week, covering a particle size range of $d \sim 1.7$–3 nm. We like to reveal the factors that control the change in specific surface area. The challenge is to elucidate the underlying mechanism of growth of the primary Fh particles at Ostwald ripening in the early stage of growth. The ultimate goal is to develop a mechanistic model for describing the time-dependent change of particle size and surface area once the initial nanoparticles have been formed. With the collected insights, we also hope to disclose the size of the initial particles, immediately after formation.

There are several approaches to assess the reactive surface area of Fh. Traditionally the specific surface area of metal (hydr) oxides is determined by probing the surface with gas molecules (N_2, Ar, and Kr). For oxides in general, it gives good results compared to other methods.[56] The BET equation is used to derive the specific surface area from the collected gas adsorption data. This method cannot be applied to assess the specific surface area of Fh nanoparticles in the wet state. Use of transmission electron microscopy (TEM) can be seen as an alternative, but the approach is experimentally challenging as fresh Fh particles are very small, usually strongly aggregated, and have a particle size distribution.[40,57–60] In case of ZnS nanoparticles, peak

broadening at X-ray diffraction has been used[34] to derive the mean particle size. The translation of size to specific surface area requires information about the particle shape,[61] while particle porosity should be unimportant.

Davis and Leckie[62] have suggested to use H^+ as probe ion to assess the specific surface area of freshly-prepared Fh. In that approach, the pH-dependent proton adsorption is interpreted with surface complexation modeling. Basic assumptions are the value of the capacitance of the inner Stern layer and the value of the molar mass of the Fh. Both are strongly size-dependent[2] but its variation can be consistently included, making the specific surface area the only adjustable parameter in a 1-p*K* approach.[27] Applying this approach to H^+ adsorption data from literature reveals a specific surface area ranging from 530–710 $m^2\ g^{-1}$ for the various Fh preparations.[27] The upper value corresponds to particles with a mean size of 2.3 nm, in agreement with TEM data for freshly prepared Fh without specific ageing.[40]

An alternative to H^+ as probe ion is the use of PO_4 ions.[2] Use of the latter has the advantage that the adsorption of PO_4 can be measured easily and accurately, since this anion has a high affinity for Fe. Comparison of the results found with proton titrations suggests good agreement[27] and is further supported by yet unpublished data. In the approach, the CD and MUSIC model recently developed for Fh has been used[2] and will also be applied in the present study.

In the present work, we will study the dynamic change of the reactive surface area of Fh kept in the wet state. We will start by producing Fh with high-speed neutralization of a Fe(III) nitrate solution with base, mixed in a flow chamber. For this material, the change of the specific surface area will be studied at a time scale between 0.1 hour and ~7 days for pH values of 5–9, maintained by means of organic pH buffer solutions, similarly as used recently by Mao *et al.*[51] In the second set of experiments, we will study the time and pH dependent ageing of traditionally produced Fh, and we will include in that study the temperature dependency (4–20 °C). The results will be compared to data for Oswald ripening of primary particles at high temperature (60–120 °C) collected with TEM.[31] For the latter data, we will show that the observed growth of the primary particles can be described with the same model that we developed for our freshly prepared Fh.

Experimental

Fh was produced by neutralizing a Fe(III) nitrate solution with NaOH, which was subsequently aged. The experiments were done in the presence and absence of organic pH buffers. In the latter case, temperature dependency was studied too. At each reaction time and pH condition, the specific surface area was measured using phosphate as probe ion. The collected PO_4 adsorption isotherms or edges were interpreted with the charge distribution (CD) and multiple site complexation (MUSIC) model of Hiemstra and Zhao,[2] making the specific surface area the only adjustable parameter. From the value of the specific surface area, the mean particle size and number of Fe ions per particle were calculated.

Ferrihydrite synthesis

High-speed neutralization. These experiments were conducted in a conditioned room (20 °C). All solutions were prepared with ultra-pure water (18.2 MΩcm at 25 °C, <1 ppb TOC) and chemical reactants of analytical grade. A mixture containing 100 mM $Fe(NO_3)_3$, 100 mM HNO_3, 38 mM MES ($C_6H_{13}NO_4S$) and 38 mM MOPs ($C_7H_{15}NO_4S$) was neutralized with 380 mM NaOH at a common tip in a tubing system and led over a glass electrode in a reaction vessel for nonstop recording of the pH (Fig. S1†). The rate of Fe addition was set to 8.0 mL min^{-1} and the rates of base addition were chosen such that the pH value remained initially ~0.5–1 pH units lower than the target value to be reached. The remaining NaOH addition (≤~5% of the total added NaOH) was done at a lower speed while magnetically stirring the suspension produced. The system was purged continuously with moist and cleaned N_2 gas. Individual batches were produced for each reaction time and pH condition. The volume of added base solution varied only slightly between individual badges prepared for systems with the same target pH (CV% of base volume <0.5%), *i.e.* the neutralization (OH/Fe ratio) was very reproducible.

For ageing, the suspensions produced were transferred into closed plastic bottles and shaken with a reciprocal shaker (180 strokes per minute). At a predefined reaction time between 0.1 hour and 7 days, the suspension was characterized with a PO_4 adsorption experiment using 6 different initial PO_4 concentrations, and the actual Fe concentration (~45 mM) was measured using Inductively coupled plasma optical emission spectrometry (ICP-OES) after dissolving a sub sample in a final concentration of 0.1 M HNO_3.

Standard synthesis of ferrihydrite. A second set of Fh suspensions was produced with our standard methodology.[2] A freshly-prepared solution of about 1.1 L containing ~3.7 mM $Fe(NO_3)_3$ dissolved in 0.01 M HNO_3 was neutralized with approximately 1.1 L of freshly-prepared 0.02 M NaOH. The initial neutralization of ~90% was done at a rate of ~200 mL NaOH min^{-1} until a pH of 3.1–3.2 was reached. Additional 0.02 M NaOH solution was subsequently added in ~5 mL increments until the suspension reached a final pH of either 6.00 (Fh pH 6) or 8.20 (Fh pH 8.2). The pH was stabilized for 15 min and next, the Fh suspensions were centrifuged at 3330*g* for 45 minutes. Subsequently, the supernatant was carefully removed and the settled Fh particles were re-suspended in a 0.0100 M $NaNO_3$ solution to a typical final volume of ~200 mL.

In some cases, the pH was slightly changed after resuspending the particles in the final background electrolyte solution. In that case, the pH was re-adjusted to the target value by using either 0.01 M HNO_3 or 0.01 M NaOH solution. These ferrihydrite suspensions were aged in a closed bottle at 20 °C for 4 hours since neutralization. Part of this stock suspension was subsequently kept at 20 °C while another part

was stored at 4 °C to determine the temperature dependency of ageing. The surface area of both suspensions was measured with PO_4 as probe ion covering the time span of 4–168 h since neutralization. The total Fe concentration of the suspensions (~20 mM) was measured by ICP-OES in a matrix of 0.8 M H_2SO_4.

Phosphate adsorption experiments

Fh systems with pH-buffer. Systems for measuring the PO_4 adsorption were prepared in 50 mL polypropylene tubes. The total volume (V_T) was 30.0 mL and typically contained ~10 mM Fe. For each pH system, a ~10 mM PO_4 stock solution was prepared by mixing Na_2HPO_4 and NaH_2PO_4 in a ratio 1 : 99 (pH 5), 1 : 9 (pH 6), 1 : 1 (pH 7), 3 : 7 (pH 8), and 7 : 3 (pH 9). Six different initial PO_4 concentrations were used ranging from ~2.3–4.5 mM at low pH, to ~1.6–3.2 mM at high pH. In addition, two systems (pH 5 and 6) with a 10 fold higher initial PO_4 concentration range were used to test the possible influence of the buffer on the PO_4-adsorption, showing no evidence for this in agreement with the work of Mao *et al.*[51] The background electrolyte solution contained ~0.10 M NO_3, 3.8 mM MES, and 3.8 mM MOPs. Equilibration was established by shaking for 16 hours at 180 strokes per minute. Equilibration for 1 hour (ref. 51) was found to be not enough. After measuring the pH and subsequent centrifugation (3750*g* for 20 min), the supernatant was filtered over a 0.45 μm filter, acidified with 1 M HNO_3 and analyzed for P with ICP-OES.

Standard Fh systems. For standard synthesized Fh, PO_4 adsorption was measured for five times of ageing at 20 °C (4, 24, 48, 72, and 166 or 168 hours), whereas for the Fh suspensions aged at 4 °C, two reaction times were used (72 and 166 or 168 hours). The phosphate adsorption experiments were done in a similar way as described above but in the absence of organic buffers and using different volumes and initial concentrations. The adsorption was measured in a background electrolyte solution of 0.01 M $NaNO_3$. Aliquots 0.01 M acid (HNO_3) or base (NaOH) solutions were added to adjust the pH values to the desired pH range of about 4–8. The final volume was 40 mL and contained 0.50 mM PO_4 and about 2.0 mM Fe. Each adsorption edge was usually composed of four evaluation points at one initial PO_4 concentration but different pH values. The final pH after equilibration for 20 hours was between pH ~ 4.2–7.6 for the series prepared with Fh pH 6 and between pH ~ 5.0–8.0 for Fh pH 8.2. All adsorption experiments were done at 20 °C. After centrifugation (3300*g* for 15 minutes) and sampling with 0.45 μm filtration, the pH was measured in the re-suspended system. The sampled supernatant was similarly analyzed for P with ICP-OES as described above. In a number of samples, Fe was also measured for verifying the quality of phase separation.

Results and discussion

Primary adsorption data

The PO_4 adsorption isotherms have been measured for Fh systems aged at pH 5.00, 6.00, 7.00, 8.00, and 9.00. The pH was stabilized during aging by a combination of organic pH buffers (~0.02 M MES and ~0.02 M MOPS). Ageing times were 0.1, 1.5, 6, 24, and 168 hours in all pH experiments except pH 7, where 24, 48, 72, and 144 hours were selected to measure the particle growth. For the systems at pH 5 and 6, the growth was also characterized by studying it with a 10-fold higher initial PO_4 concentration (~15–35 mM). Fig. 1 gives two examples of the decrease of the PO_4 adsorption isotherm with ageing. The trend of decrease with time of ageing is very similar in both cases. For pH 5, the P/Fe ratios are much higher than for pH 8, but this is mainly due to less PO_4 adsorption at higher pH values as follows from CD modeling. Initially, all particles are very small. The PO_4 adsorption is roughly halved during 168 hours of ageing, suggesting a change of the surface area by a factor of about 2.

CD MUSIC modelling

The adsorption measured in the various systems can be described with the CD model. Previously, the PO_4 adsorption has been studied extensively[2] and the resulting parameter set has been applied to describe the present data sets. In this approach, the reactive surface area is the only adjustable parameter and its value can be found by fitting the measured PO_4 adsorption isotherms. However, for a proper interpretation, the molar PO_4/Fe ratio needs to be translated into the PO_4 adsorption per unit mass of Fh. This requires

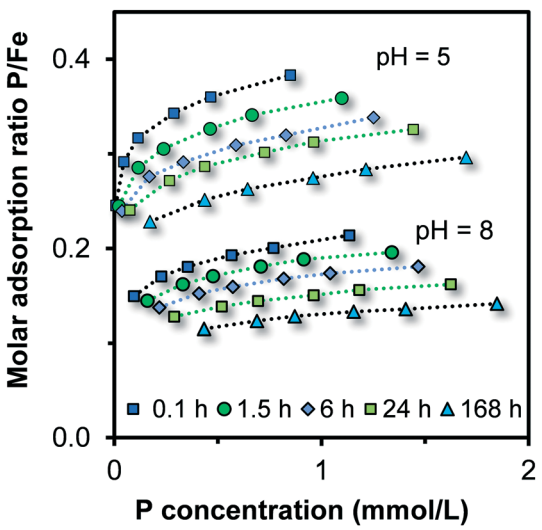

Fig. 1 Time-dependent PO_4 adsorption isotherms in ~0.10 M $NaNO_3$ measured at pH 5.38 ± 0.12 and 8.01 ± 0.21 buffered with 3.8 mM MES and 3.8 mM MOPS (symbols). The Fh was formed and aged at pH 5.00 and 8.00 (20 °C) in solution containing finally ~0.10 M $NaNO_3$, ~19 mM MOPS, and ~19 mM MES. The lines have been calculated with the CD model, taking for each individual data point the corresponding experimental pH and total concentrations of Na, NO_3, PO_4, MES, MOPS, and Fe. The molar masses of Fh were found iteratively with CD modelling from the fitted specific surface area *A* (eqn (1)). With time, it typically decreased from M_{nano} ~ 107 to ~94 g mol^{-1} Fe.

the value of the molar mass. The latter is not constant, but depends on the (yet unknown) specific surface area. The molar mass of the nanoparticle M_{nano} (g mol^{-1} Fe) is a function of the specific surface area A (m^2 g^{-1}) and the excess surface water density N_{H_2O} (12.6 10^{-6} mol m^{-2}), as derived previously.[29,63]

$$M_{nano} = M_{core} \frac{1}{\left(1 - A\, N_{H_2O} M_{H_2O}\right)} \quad (1)$$

The reason for a variable molar mass is the presence of surface groups that lead to a change of the molar composition.

The molar composition of Fh can be given as $FeO_{1.4}(OH)_{0.2}.nH_2O$ in which n is the molar amount of chemisorbed water in excess to the bulk composition $FeO_{1.4}(OH)_{0.2}$. This excess amount of coordinated water (n) can be calculated from the difference in the molar mass of the nanoparticle (M_{nano}) and mineral core or bulk (M_{core}), scaled to the molar mass of water M_{H_2O}, according to:

$$n = \frac{M_{nano} - M_{core}}{M_{H_2O}} \quad (2)$$

The molar mass M_{nano} (g mol^{-1}) and surface area A (m^2 g^{-1}) are iteratively found in a cycle of CD modeling and recalculation of the PO_4 adsorption per unit mass (mol kg^{-1}) from the primary PO_4/Fe ratio, and this is used to generate a new input for the fitting procedure. In this process, the values of the Stern layer capacitances are also continuously adapted to account for the surface curvature of the spherical particle with a diameter d calculated from the corresponding specific surface area A. In Fig. S2,† the influence of the surface curvature on the PO_4 adsorption is shown.

The translation from A (m^2 g^{-1}) to d (m) requires the value of the mass density of the nanoparticle ρ_{nano} (g m^{-3}), which is variable since the amount of coordinated water (n) adds more to the volume than to the mass of the particle. The relationship between the mass density and molar mass of a nanoparticle can be given as:

$$\rho_{nano} = \frac{M_{nano}}{V_O \times \left(n_O + n\right)} = \frac{M_{nano}}{V_O \times \left(n_O + \left(M_{nano} - M_{core}\right)/M_{H_2O}\right)} \quad (3)$$

in which V_O is the lattice volume of Fh per oxygen in m^3 per mole oxygen ions, n_O is the number of oxygens per Fe in the bulk of Fh (1.6) and n is the amount of excess water defined in eqn (2).

In the above approach, the primary PO_4 adsorption data of Fh in the various systems have been used to derive the specific surface area. In a self-consistent manner, the effect of surface curvature is also included by translating the surface area to the corresponding spherical particle diameters d (m) according to:

$$d = \frac{6}{\rho_{nano} A} \quad (4)$$

The corresponding number of Fe ions in the particle (n_{Fe}) follows from:

$$n_{Fe} = \frac{\rho_{nano}}{M_{nano}} \frac{\pi d^3}{6} N_{Av} \quad (5)$$

in which N_{Av} is Avogadro's number.

The above-described theoretical relation between chemical composition and particle size is shown for Fh in Fig. 2 (line) together with experimental data (blue spheres) of Michel *et al.*,[40] as well as data derived by constructing Fh particles with Crystalmaker® (open squares) with a procedure described previously.[33,64] Good agreement exits between model and data, which implicitly indicates the correct calculation of molar mass M_{nano} and mass density ρ_{nano}.

At very low pH (<2), small angle X-ray scattering (SAXS) points to the formation of ultra-small nuclei.[48] The reported

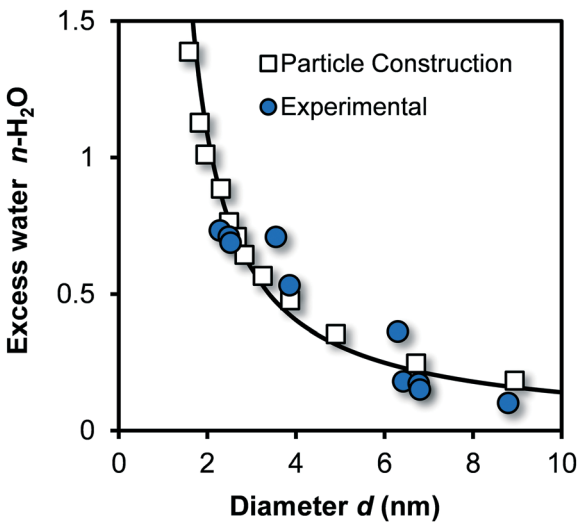

Fig. 2 Excess water (n) of Fh ($FeO_{1.6}H_{0.2}.nH_2O$) as a function of particle size. The blue spheres are data collected by Michel *et al.*[40] for a series of Fh particles aged at high temperature. The mean diameter has been found with high-resolution transmission electron microscopy (HR-TEM). The white squares have been derived by constructing near-spherical Fh particles from which all Fe_2 and Fe_3 were removed that formed singly coordinated surface groups.[33,64] The corresponding size was calculated based on the number of oxygen in the particle and the value for lattice volume expressed per oxygen V_O (107 10^{-6} m^3 mol^{-1}). Using the principle of electro neutrality, the total number of H can be found for each particle from which one gets the excess number of protons by subtracting the number of structural H according to the composition $FeO_{1.4}(OH)_{0.2}$. It yields the corresponding amount of coordinated surface water. The model line is calculated applying eqn (1)–(4), showing good agreement with the data.

Fe-dominated radius of r_o = 0.41 nm translates to a particle size by incorporating an effective O diameter of about ~0.20–0.25 nm, leading d ~ 1.22–1.32 nm, in agreement with our equivalent spherical diameter of ~1.25 nm calculated for Fe_{13}. A neutral Fe_{13} cluster will have a chemical composition of $Fe_{13}O_{40}H_{41}$. Compared to the bulk composition of Fh, the excess amount of coordinated water is n_{H_2O} = 2.9, which is extremely above any of the values for excess water of Fh particles, given in Fig. 2. It indicates that the Fh structure is significantly more condensed than any collection of aggregated Fe_{13} clusters. The core–shell structure suggested for the Fh[48] is in line with the particle size dependency of the ferrimagnetic behavior of Fh as shown recently.[33] Other SAXS data[59,60] for characterizing Fh will be discussed later.

Particle evolution with time

In Fig. 3, the pH and time dependent evolution of Fh is given showing the specific surface area A, the mean particle diameter d, and the number of Fe per particle n_{Fe} (symbols), obtained by interpreting the primary PO_4 adsorption data collected at the various pH values and times of ageing at 20 °C. At the logarithmic time scale, the measured specific surface area decreases almost linearly. After a few minutes of ageing, the particles are still very small. Depending on the pH, A = 1100–900 $m^2\ g^{-1}$, d = 1.7–1.9 nm, and n_{Fe} = 50–80.

Rate of growth

To get insight into the process of growth during Ostwald ripening, the data require rescaling to reveal the rate of growth that allows deriving the underlying rate law.

At particle growth, there is a flux of Fe towards the surface. This flux (mol h^{-1}) can be expressed per unit surface area (mol m^{-2} h^{-1}). To do this scaling, the data have been described with a mathematical trial function that can excellently depict the evolution of the particle size (d) with time of ageing (t). The equation used is $d = at^{1/n} + d_o$ in which the parameters a, d_o, and $1/n$ are derived by fitting. This can be done conveniently by plotting the diameter d against the time parameter ($t^{1/n}$), evaluating linearity by searching for the best value of the exponent $1/n$ (Fig. S3†). The correlation coefficients obtained are very high ($R^2 \geq 0.99$), *i.e.* this linear relationship describes the time dependency very well.

The parameterized trial functions can be used to calculate the rate of growth at the various times of ageing by taking the derivative ($\partial d/\partial t$) that also allows the calculation of the change of the number of Fe per particle (n_{Fe}) with time ($\partial n_{Fe}/\partial t$). By scaling to the corresponding surface area (m^2) of the particle ($A_\# = \pi d^2$), one derives the rate of growth R expressed as the number of Fe ions that become attached per unit surface area and time *i.e.* $R = (\partial n_{Fe}/\partial t)/A_\#$ with the unit μmol m^{-2} h^{-1}. At each reaction time, it represents the Fe-flux towards one unit of surface area. This rate of particle growth R is shown in Fig. 4 as a function of time for the various systems studied.

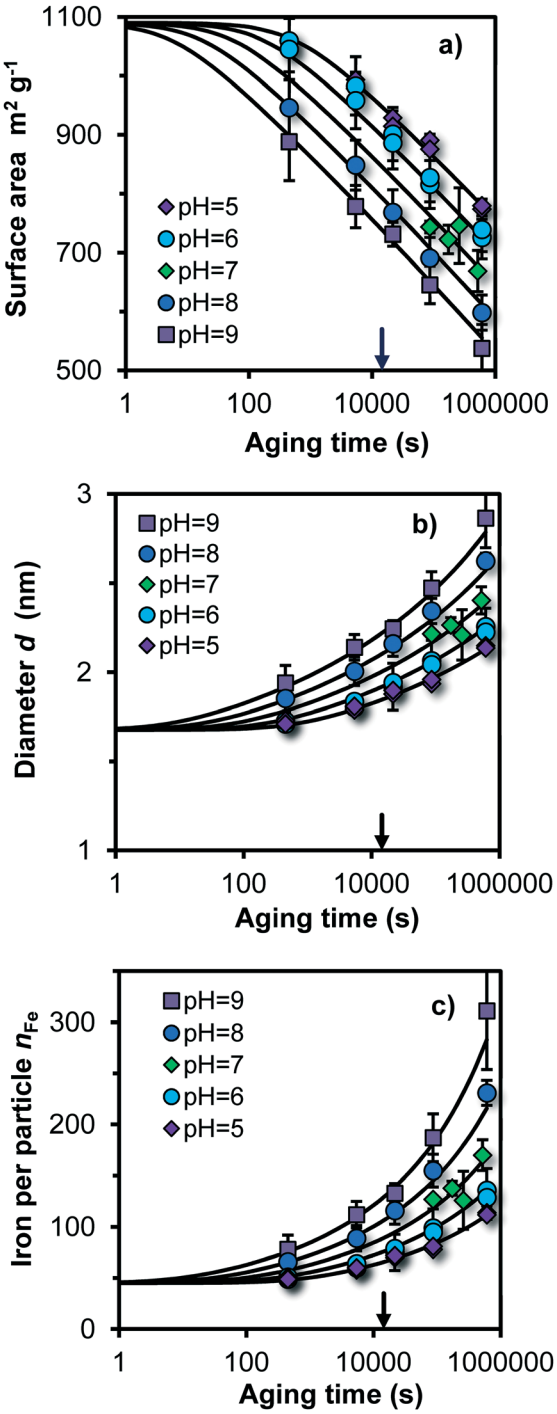

Fig. 3 a) Evolution of the specific surface area (A), b) mean particle diameter (d), and c) number of Fe per particle (n_{Fe}) as a function of the logarithm of the ageing time for Fh produced and aged at 20 °C in a solution with 0.2 M $NaNO_3$, 19 mM MOPS, and 19 mM MES with pH values as indicated. The lines have been calculated with the dynamic simulation model presented and discussed using eqn (9) as rate law with $\log k_0$ = 4.80 (m^{-2} s^{-1}) or $\log k_0$ = −9.58 (μmol m^{-2} s^{-1}) and a = −0.5. The arrow at the x-axis indicates the ageing time of 4 hours that is often used in ion adsorption experiments with Fh.

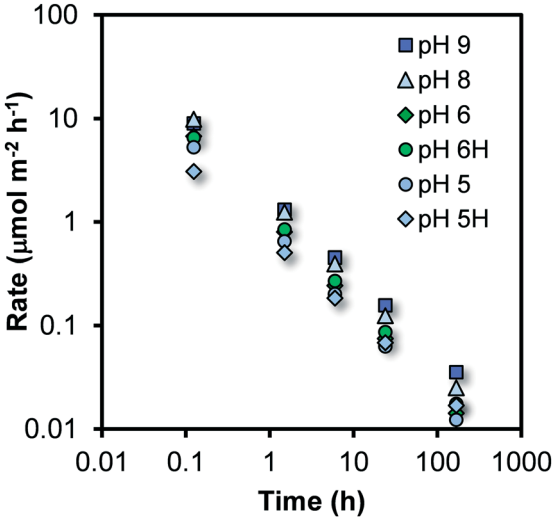

Fig. 4 Development of the rate of growth R with time for 30 Fh materials prepared and aged (20 °C) at the various pH values indicated. The rate of Fe growth continuously decreases and changes by near three orders of magnitude for the time range studied. The change of the rate of growth is very similar for the Fh systems of different pH. For the systems pH5H and pH6H, the results have been obtained using a 10-fold higher PO_4 addition to measure the surface area.

Rate limiting step

It is obvious from Fig. 4 that the rate of growth R is not constant. Initially, it is around 3–10 μmol m^{-2} h^{-1} but decreases dramatically by nearly three orders of magnitude during the course of the experiment. At the highest measured rates, the particles grow with less than one monolayer of Fe polyhedra per hour, as the Fe density of the Fh surfaces is 15–20 μmol m^{-2} (Fig. S4†). However, our dynamic model suggests significantly higher rates immediately after the formation of the initial, yet non-aged, particles (scale of seconds).

As mentioned, the Fe-flux towards the surface becomes substantially less with time. Considering the process of growth as a chemical reaction of Fe in solution with specific reactive surface sites, the decrease of the rate of growth suggests that the solution concentration of Fe is considerably changing since the reactive site density can be seen as an intrinsic surface property of Fh.

At a given pH, the concentration of Fe in solution will be a function of the solubility product of Fh (Q_{so}). The solubility of nanoparticles is enhanced relatively to the intrinsic solubility of the bulk material (K_{so}). In a suspension with a given particle size distribution, the solubility is determined by a labile equilibrium between Fe in solution and particles in the critical state having the highest Gibbs free energy.[29] All particles larger than the critical ones will have a lower chemical potential, a higher stability, and consequently, a lower solubility. For this reason, the vast majority of particles will grow, which will be at the expense of the smallest particles that dissolve in an attempt to maintain the solution concentration. This is the driving force for Ostwald ripening. The rate-limiting step of growth is the binding of Fe to the surface because the rate of dissolution of the smallest particles is sufficiently high to maintain an equilibrium concentration in the solution.

The solubility of the critical nuclei of Fh with a surface area A_{crit} (m^2 g^{-1}) can be described with the Ostwald–Freundlich equation, according to:

$$RT \ln \frac{Q_{so}}{K_{so}} = \frac{2}{3} M_{nano} \gamma A_{crit} \quad (6)$$

in which Q_{so} is the activity product that we define as $Q_{so} = (Fe^{3+})\,(OH^-)^3$ and K_{so} is the corresponding intrinsic value for the virtual bulk, being $\log K_{so} = -40.6 \pm 0.2$ (ref. 29) in agreement with calculations of Pinney *et al.*[65] Furthermore, M_{nano} is the molar mass (eqn (1)), R is the gas constant, and T is the absolute temperature. For Fh, the surface Gibbs free energy γ (J m^{-2}) has recently been derived by Hiemstra[29] interpreting a set of thermochemical data of Majzlan *et al.*[66] and Snow *et al.*[67] The value of the surface Gibbs free energy is exceptionally low ($\gamma = 0.186 \pm 0.01$ J m^{-2}) compared to the values for all other Fe (hydr)oxides.[68] It indicates that the surface of Fh has a relatively high stability, which can be explained by the absence of unstable Fe2 and Fe3 polyhedra at the surface according to the surface depletion model.[29] We assume that the value of γ is particle size independent, based on recent results obtained from silver nanoparticles.[69]

As follows from TEM data,[40,58] freshly prepared Fh has a particle size distribution in which the mean and minimum particle sizes are linearly correlated.[29] Introducing the ratio $\phi \equiv A_{crit}/A_{mean}$ between the specific surface area of the measurable mean (A_{mean}) and critical (A_{crit}) particle (m^2 g^{-1}), the Ostwald–Freundlich equation can be rewritten to:

$$RT \ln \frac{Q_{so}}{K_{so}} = \frac{2}{3} \phi M_{nano} \gamma A_{mean} \quad (7)$$

Eqn (7) shows that the super saturation of a solution relatively to the bulk material of infinite size (Q_{so}/K_{so}) is related to the mean specific surface area of Fh material (A_{mean}). This relation will be used in our derivation of the rate law of particle growth at Ostwald ripening. Analysis of the TEM data of Michel *et al.*[40] reveals a factor $\phi = 3/2$.[29] The same conclusion follows from the data of Burrows *et al.*[58] Introducing this information ($\phi = 3/2$) in the above Ostwald–Freundlich equation (eqn (7)) leads to an equation without the factor 2/3 ϕ, known as the Ostwald equation.[29]

Rate law

As pointed out above, the process of growth can be considered as the attachment of dissolved Fe to reactive sites at the surface of Fh having a certain Fe-reactive site density N_r (mol m^{-2}). Since the solubility of Fh can be related to the mean specific surface area A (eqn (7)), a relation between the rate of growth R and the ratio for super saturation Q_{so}/K_{so} is expected. In Fig. 5, the growth rate R has been related to Q_{so}/K_{so} by plotting both on a logarithmic scale. The data for pH 7

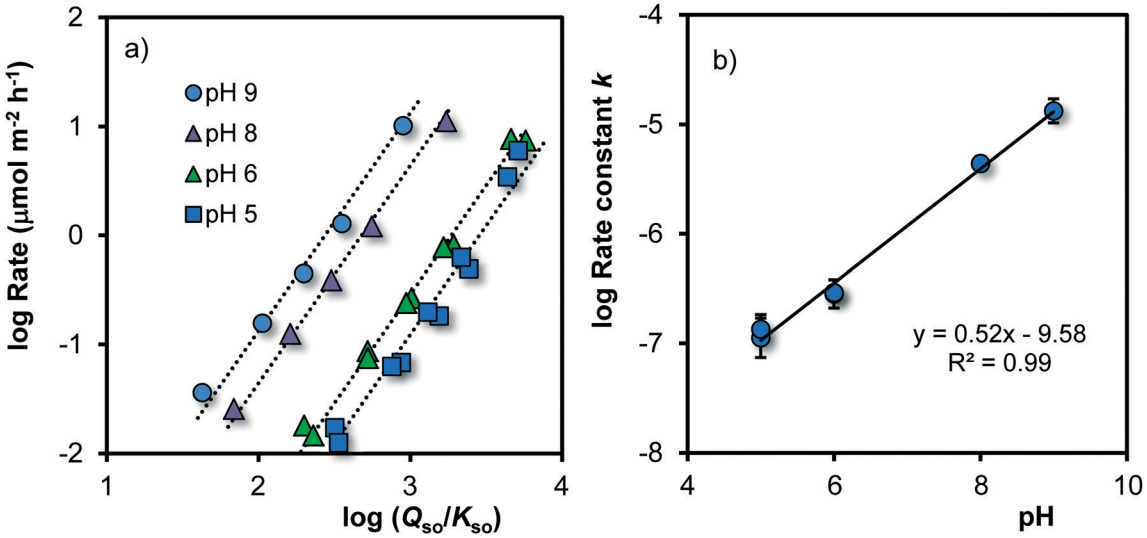

Fig. 5 a. Logarithm of the rate of growth R (μmol m^{-2} h^{-1}) as a function of the logarithm of the super saturation of the solution (Q_{so}/K_{so}) for Fh in 0.2 M $NaNO_3$ buffered with 19 mM MES and 19 mM MOPS at the given pH values (T = 20 °C). The slopes of the calculated lines (s) have been set to s = 2. The intercept at $\log(Q_{so}/K_{so})$ = 0 equals the logarithm of the rate constant ($\log k$), which is plotted in Fig. 5b against the pH, revealing the pH dependency of $\log k$ (eqn (8)) with k in μmol m^{-2} h^{-1}.

have been omitted in this part of the analysis, because the time scale of the measurement is too limited due to the absence of data for short ageing times.

Fig. 5a shows that the rate of growth varies with the super saturation of the solution (Q_{so}/K_{so}). Initially, the super saturation is typically ~1.000–10.000 ($\log Q_{so}/K_{so}$ = 3–4). After a few minutes of ageing, the mean size is 1.8 ± 0.1 nm and the corresponding solubility is about $\log Q_{so}$ ~ −37.2 ± 0.3, which matches within the uncertainties with the solubility ($\log Q_{so}$ ~ −37.5 ± 0.1) at rapid titration of Fe(II)/Fe(III) solution with NaOH in $NaClO_4$, back calculated to pH = PZC from the measured free [Fe^{3+}] concentration.[70]

The data in Fig. 5a reveal a mean slope of s = 1.97 ± 0.18, which implies that within the uncertainty, the rate of growth R (μmol m^{-2} h^{-1}) is proportional to the square of the super saturation (Q_{so}/K_{so}). Therefore, the rate can be described with the conceptual equation:

$$R = k_r N_r \left(\frac{Q_{so}}{K_{so}}\right)^2 \equiv k \left(\frac{Q_{so}}{K_{so}}\right)^2 \quad (8)$$

in which k_r is a reaction constant (h^{-1}) and N_r is the Fe-reactive site density of the surface (μmol m^{-2}). The precise value of the latter is unknown and therefore, it is combined with k_r to the pre-factor k (μmol m^{-2} h^{-1}).

The observation of a quadratic relation between rate and solubility can be interpreted as rate limitation by a site binding reaction of two Fe with one site (S + 2 Fe → SFe_2). The rate-limiting step is the simultaneous attachment of two Fe species forming together a stable surface complex. The value of 2 for the exponent of Q_{so}/K_{so} expresses the chance that two Fe species occupy simultaneous a single site of growth, resulting in a stable complex. If only one monomeric Fe species is attached, it may be labile and desorb again in dynamic events, while the binding of two Fe ions, *i.e.* formation of an adsorbed Fe-dimer, may be irreversibly. Possibly, the formation of the adsorbed Fe-dimer is *via* the attachment of individual Fe-monomers since aqueous Fe-dimers are typically formed at high total Fe-concentrations present in systems with very acidic conditions (pH ~ 2), as confirmed experimentally.[49,50]

In Fig. 5a, the intercept at the y-axis is equal to $\log k$ of eqn (8). That intercept is pH dependent. The pH dependency of $\log k$ can be revealed by plotting its value *versus* pH (Fig. 5b). To reduce the interrelation between the intercept value and the slope (s) of the lines in Fig. 5a, the latter has been fixed to $s \equiv 2$. Incorporating the obtained pH dependency of the rate constant, we can rewrite eqn (8) to:

$$R = k_0 \left(H^+\right)^a \left(\frac{Q_{so}}{K_{so}}\right)^2 \quad (9)$$

in which k_0 is a pH-independent rate constant and the exponent a determines the dependency of the growth rate R on the proton activity (H^+). The data of Fig. 5b suggest a = −0.5.

Dynamic modelling

The above-derived rate law for Ostwald ripening of primary Fh particles in a suspension can be applied in dynamic modeling by defining a flux of Fe towards the surface of an Fh nanoparticle of certain mean size (d) and surface area of $A_\# = \pi d^2$. The Fe flux F (mol h^{-1}) can be related to the rate of surface growth of the particle R (mol m^{-2} h^{-1}), according to:

$$F = RA_\# \quad (10)$$

in which the surface area $A_\#$ has the unit m^2. In our dynamic model, the rate of growth R is described with the rate law

(eqn (9)) that has been derived with the above data analysis (Fig. 5). The results of these simulations are shown in Fig. 3 with lines.

At each (small) time step (Δt) in the modeling, the total number of Fe in the particle (n_{Fe}) has been calculated according to $n_{Fe} = n_{Fe(t=0)} + \Sigma\, \Delta n_{Fe}/\Delta t$. Additionally, a corresponding set of related parameters was calculated, *i.e.* the molar mass M_{nano} (g mol^{-1}), mass density ρ_{nano} (g m^{-3}), diameter d (m), particle surface area $A_{\#}$ (m^2), and the specific surface area $A_{mean} = N_{Av}/(n_{Fe}M_{nano})\ A_{\#}$ (m^2 g^{-1}). Combining the latter with the surface Gibbs free energy γ (J m^{-2}) and molar mass M_{nano} (g mol^{-1}) allows the calculation (eqn (7)) of the relative solubility Q_{so}/K_{so} (ϕ = 3/2), which is subsequently applied in the rate equation (eqn (9)) to find $\Delta n_{Fe}/\Delta t$ before calculating the next time step.

In the modeling approach, the initial particle size at t = 0 is an adjustable parameter. Application of the model shows that we can describe the evolution of the size and specific surface area of the particles using a single value for the number of Fe present in the initial particle, independent of the pH. The data indicate that the non-aged particle (made at room temperature) has an equivalent spherical size of $d \sim$ 1.68 nm and a corresponding Fe content of $n_{Fe} \sim 45$. One may construct such a representative particle by linking two Fe_{13} moieties and extend it with attaching additionally Fe polyhedra in accordance to the surface depletion model as given in Fig. S5.†

For different pH values, we find at the first sampling point (t = 0.1 h) a significant difference with the calculated initial size at t = 0. At pH = 9, $n_{Fe} \sim 80$, while for pH = 5, $n_{Fe} \sim 50$ for t = 0.1 h. The reason for this difference is the variation in the rate of growth. The model curves in Fig. 3c show that practically no difference exits in the calculated number of Fe per particle (n_{Fe}) at the typically time scale of about a second. This is also the time scale of physical mixing of the Fe(III) and base solution in the flow chamber. The differences in size observed at the first sampling point, a few minutes after the formation, are due to differences in rate of growth by Ostwald ripening, being relatively high at pH 9 and low at pH 5. We note that the data for the first sampling point at t = 0.1 h are potentially affected by the kinetics of the adsorption of PO_4. However, one may expect that the added PO_4 will promptly stop the ageing process when adsorbed, even though full equilibration[2] may take more time.

Visual inspection of the process of formation in a flow chamber and connected tubing system shows a rapid change in color from pale-yellow to a yellow-brown upon mixing of the reactants. In the next seconds, the transparency changes and one starts to observe the formation of aggregated, reddish-brown Fe (hydr)oxide that contains micro-aggregates with a size of about 50 nm or larger.[48,60,71] Formation of loose flocs (~mm) in the tubing system is almost complete in less than 30 seconds. These observations illustrate the ultra-high speed of the formation reaction of Fh and the subsequent very fast physical process of aggregation and floc formation.

Ageing of transitionally synthesized Ferrihydrite

Above, we find that flash neutralization of Fe(III) in a pH-buffered solution leads to the synthesis of relatively small particles that reach a specific surface area of 750–950 m^2 g^{-1} after ageing for 4 hours (Fig. 3a). These values are significantly higher than the typical values of 530–710 m^2 g^{-1} found with the classical synthesis of 2LFh described in literature.[27] This difference is an important motivation to extend our work by including Fh synthesized with the traditional approach of Fe(III) neutralization.

To extend the lifetime of freshly prepared two-line Fh (2LFh), researchers have stored their suspensions at low temperature in a refrigerator. Therefore, we have also studied the ageing at 4 °C to derive the temperature dependency of the particle growth. Our results refer to a single 2LFh material made by neutralizing a 3.3 mM Fe(III) nitrate solution with a 0.02 M NaOH solution to a pH value of pH 6.0 or 8.2 and an initial ageing for 4 hours since neutralization. After sampling, the ageing was continued at temperatures of either 4 °C or 20 °C. The experimental results are shown in Fig. 6.

Analysis of the data of particle growth at pH 8.2 along the same lines as presented above (Fig. 5) revealed that the rate dependency of the particle growth is basically the same as in the systems of Fig. 3, in the sense that the exponent for the dependency on the solubility is the same, *i.e.* $R \propto (Q_{so}/K_{so})$.[2] It strongly suggests that the ageing process has the same rate-limiting step as found above, *i.e.* a dual attachment of Fe.

When the dynamic model was applied, we found that we can use the same value for the initial size of the non-aged primary Fh particles (n_{Fe} = 45) as in the experiments with the formation of Fh in the flow chamber in the presence of organic pH buffers. However, a somewhat higher value is also possible as our data only refer to a relatively long time of ageing (≥4 h), making the approach less sensitive to pinpointing the precise initial value at t = 0. This is illustrated in Fig. S6,† showing that an increase of the initial size hardly affects the particle size at a longer time of ageing (>day). The modeling of Fig. S6† also shows that it is difficult to grow Fh particles to sizes larger than ~3–4 nm by the process of Ostwald ripening at room temperature and circumneutral pH values. However, additionally growth will occur by oriented attachment.[31]

Evolution of ferrihydrite according to TEM

The growth of Fh can also be studied by directly observing the change in particle size with TEM. This was done by Burleson and Penn[31] studying the ageing of Fh for 20–2000 h as a function of temperature (60, 90, and 120 °C) and pH. The initial Fh sample was prepared by neutralizing a Fe(III) solution with $NaHCO_3$, followed by dialysis at 4 °C during 5 days with a final pH of ~ 3.5. The created particles have a mean diameter of 3.0 nm (black square in Fig. 7a), and will contain about 360 Fe.

The TEM data of Burleson and Penn[31] show the simultaneous presence of relatively small primary particles as well as larger particles with another aspect ratio (~5) that have

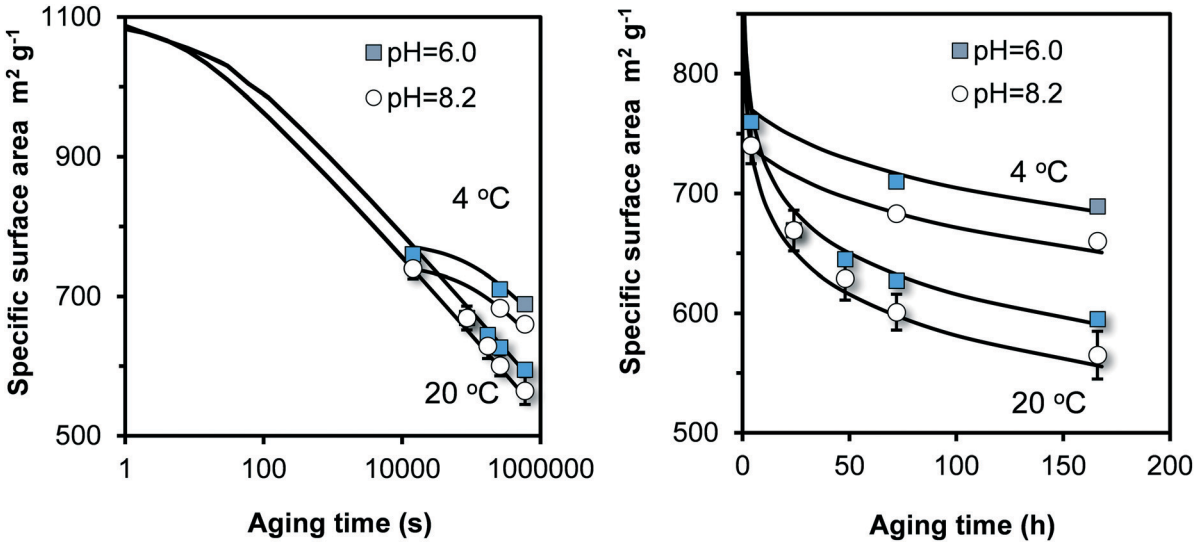

Fig. 6 Time dependency of the specific surface area ($m^2\ g^{-1}$) for traditionally synthesized Fh, aged in 0.01 M $NaNO_3$ in the absence organic pH buffers. After synthesis at pH 6.0 or 8.2, the Fh materials were aged for 4 hours since neutralization before a first sample was taken. The remaining suspensions were split and further aged at either 4 °C or 20 °C. The lines have been calculated with the model (eqn (8)), only adjusting the rate constant k. At 20 °C, $\log k$ = 9.25 (pH = 8.2) and 9.00 (pH = 6), and at 4 °C, $\log k$ = 8.35 (pH = 8.2) and 8.10 (pH = 6) with k in Fe per m^2 per second. Subtracting a value of 14.22 from these $\log k$ values gives $\log k$ in the unit $\mu mol\ m^{-2}\ s^{-1}$.

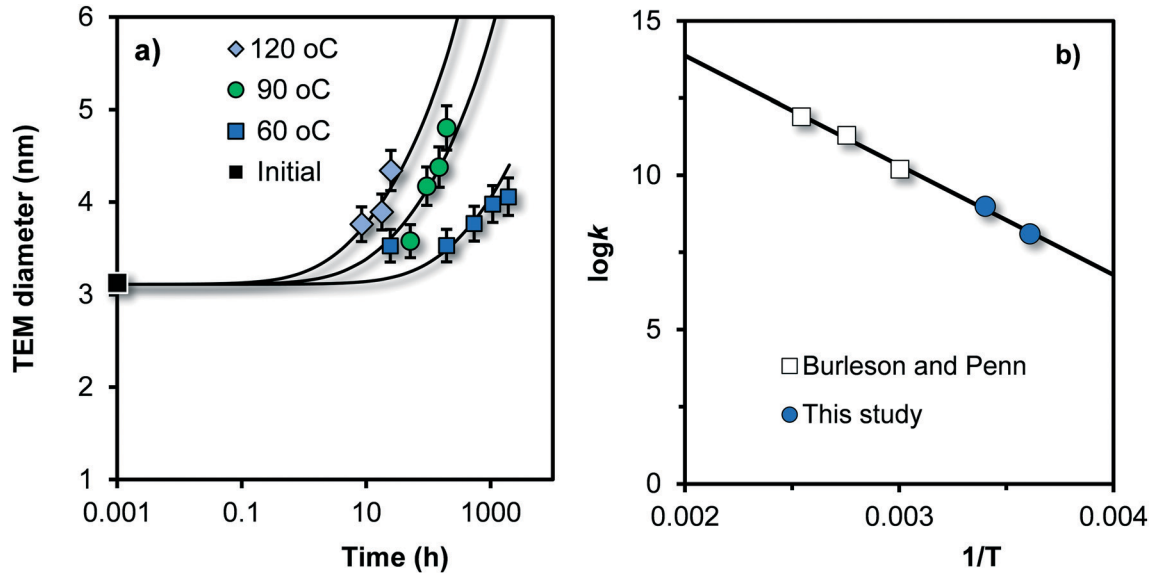

Fig. 7 a) Time dependency of the mean size of primary particles in Fh suspensions, measured with TEM at pH = 6 by Burleson and Penn[31] for different temperatures (symbols). The data only refer to the fraction of primary particles in the suspension, excluding the particles that formed by oriented particle attachment. The k value (eqn (8)) in Fig. 7b) is given in the unit Fe per m^2 per second. The slope to the line is equivalent to an activation energy of E_{act} = 68 ± 4 kJ mol^{-1} (see text).

formed by oriented attachment, particularly at pH ~ 10–12. However, the data in Fig. 7a refer only to the growth of the fraction of primary particles. The other particles have been excluded and were evaluated differently by Burleson and Penn.[31] With increase of temperature, the rate of growth of the primary particles increases. Despite the high temperature, the Ostwald ripening of these particles is still relatively slow. At 120 °C, the mean diameter increases with only ~0.5–1.5 nm in one day.

Fh particles can also grow by oriented attachment.[31] This typically occurs at high temperature, similarly as found for ZnS.[34] Oriented attachment of Fh may occur once the particle size of Fh is large enough to develop preferred crystal faces. Ferrihydrite, hydrothermally aged at 175 °C,[40] shows a rapid near-doubling of the mean particle size as soon as the particles reach a mean size of about 3.5–4 nm.[33] Simultaneously, the magnetic saturation becomes less than expected for defect free Fh,[33] which suggests imperfect attachments. Upon

further hydrothermal ageing, the reduction of the magnetic saturation (*i.e.* defects) gradually disappears, signifying completion of the particle fusion. These particles are large enough (~8 nm[29]) to transform into hematite.[40]

The TEM data (symbols) of Fig. 7a have been described with our kinetic model (lines) by only adjusting the rate constant k of eqn (8) while using the reported experimentally value (3 nm) as initial particle size. These rate constants have been given as open squares in Fig. 7b as a function of the inverse of the temperature ($1/T$). The k value is given in the unit m^{-2} s^{-1} but can be expressed in μmol m^{-2} h^{-1} using Avogadro's number and 1 h = 3600 s. The blue spheres in Fig. 7b refer to the $\log k$ values obtained from our data collected at the same pH (pH = 6) in 0.01 M $NaNO_3$.

Temperature dependency

The temperature dependency of the rate constants k obtained by modeling (Fig. 7b) can be described with the classical Arrhenius equation:

$$k = Ae^{-E_{act}/RT} \quad (11)$$

in which A is a pre-exponential factor related to the frequency and E_{act} is the energy of activation (J mol^{-1}). If applied to the overall rate constant k for particle growth of Fh at pH = 6 (Fig. 7b), assuming no other factors of temperature dependency, it provides an apparent energy of activation of E_{act} = 68 ± 4 kJ mol^{-1}. This activation energy is of the same order as found in literature for the conversion of Fh to goethite (52 ± 4 kJ mol^{-1}) at high pH (12) and the dissolution of various Fe oxides in hydrochloric acid (67–94 kJ mol^{-1}) as summarized by Cornell and Schwertmann.[28] Growth by oriented attachment is more temperature dependent than growth by Ostwald ripening, *i.e.* has a higher activation energy,[34] and ion diffusion in water is less temperature dependent.

Time dependency

Burleson and Penn[31] have previously used the classical model of Lifshitz and Slyozov[72] to evaluate the growth of the primary Fh particles. In that model, the rate of growth is limited by the diffusion of Fe between the free solution and particle surface. In the model, the Ostwald–Freundlich equation is linearized which is increasingly justified for systems with little supersaturation (Fig. S7†). For a polydisperse system, Lifshitz and Slyozov[72] derived that the particle volume increases linearly with time ($\Delta V_{mean} \propto t$). This increase is equivalent to a time-dependent change of the particle diameter according to $\Delta d \propto t^{1/3}$. However, our data do not show this time dependency. It can be shown that the growth of Fh is likely not limited by diffusion across the solid–solution interface (Fig. S8 and Table S1†). The process is much slower.

For a polydisperse system, Wagner[73] derived a time dependency of the mean size of $\Delta d \propto t^{1/2}$ if the growth is limited by a chemical reaction that is first order in concentration (c^1). In case of a surface reaction that is second order with respect to the concentration (c^2), the rate will be more time-dependent. Our data analysis and model suggest $\Delta d \propto t^{1/n}$ with n = 3.9 ± 0.7 (Fig. S3†), *i.e.* approximately $\Delta d \propto t^{1/4}$. Remarkably, the theoretical growth of lens-shaped particles at the boundary between two matrices may exhibit the same time dependency,[74] indicating that time dependency should be interpreted with care.[34]

Six-line Fh (6LFh) can be made by forced hydrolysis at 75 °C in about 10–12 minutes[25] without base addition. It leads to particles with a size of ~5.5 nm according to TEM[57] and SAXS.[59] If formed by prompt adsorption of Fe to Fe_{13} nuclei, about 7 ± 1 monolayers of Fe polyhedra are needed (Fig. S4†). This assumption implies less nucleation in the solution than at the formation of 2LFh by Fe(III) neutralization with base at room temperature. The 6LFh particles with d = 5.5 nm typically contain n_{Fe} ~ 2600 Fe. Further growth by classical Ostwald ripening will be little at room temperature according to our model (Fig. S9†). This is due to the very low solubility of these particles and super saturation ($\log Q_{so}/K_{so}$ ~ 0.6) of the solution. Indeed, no ageing occurs during storage for months at room temperature, according to SAXS.[59] Apparently, oriented attachment or particle fusion does not play a significant role in that case.

pH dependency

The logarithms of the rate constants, $\log k$ (eqn (8)), for Fh aged in the absence and presence of organic pH buffers are compared in Fig. 8. At low pH, the rate constants for growth are much lower in the presence of organic pH buffers (MES and MOPS), resulting in a larger pH-dependency. At low pH, the rates constants are strongly reduced compared to Fh systems without these organics. It suggests that at low pH the organic molecules are present at the surface, hindering the process of Fe adsorption. The interaction of these organic molecules with the surface will be relatively weak since these ions do not influence the adsorption of PO_4 at the concentration scales studied.[51] These organic molecules are negatively charged in the pH range studied (At 20 °C and I = 0.1 M, log K_H = 6.16 for MES add $\log K_H$ = 7.17 for MOPS) and may interact by electrostatic forces with the positively charged surface groups at a pH below the value of the PZC (~8.2). At higher pH, the interaction will largely disappear leading to the same rates as in the pure Fh systems.

Role of organic matter and anions

The above indicates that any disturbance of the Fe attachment by the presence of organic molecules may highly reduce the rate of growth and transformation. As organic matter is readily available in nature, it implies that Fh particles may have significantly lower rates of transformation in the natural environment. This will contribute to the nano-character of the natural iron oxide fraction of many top soils.[75] The primary iron and aluminum (hydr)oxide particles remain ultra-small, and are embedded in and/or covered by organic matter, since

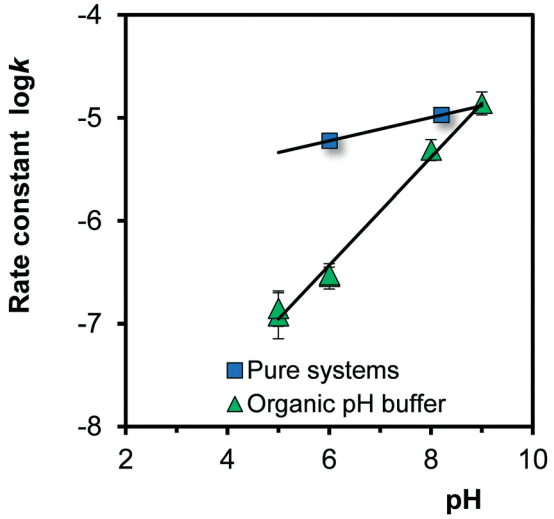

Fig. 8 pH dependency of the rate constant of growth of Fh at 20 °C ($\log k$ of eqn (8) with k in μmol m^{-2} h^{-1}) in the absence (squares) and presence (triangles) of an organic pH buffer solution. In the latter case, the rate is strongly reduced at low pH, which can be explained by a weak interaction of the organic molecules with the surface.

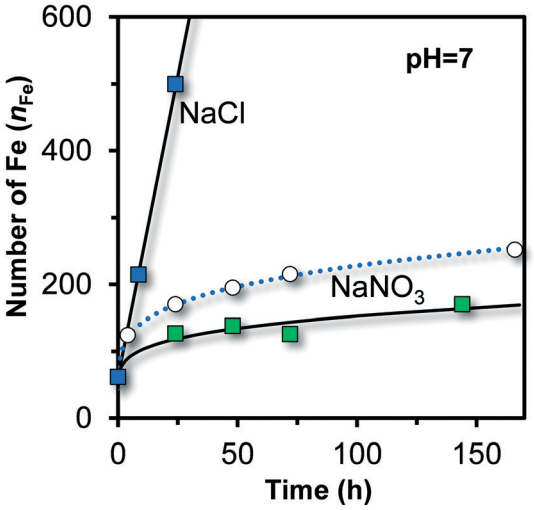

Fig. 9 Ageing of ultra-fast synthesized Fe (hydr)oxide in 0.1 M NaCl (ref. 51) and 0.1 M $NaNO_3$ (present study) at pH = 7 in the presence of organic pH buffers (squares). The reaction pathways start to deviate significantly after ~4 hours of ageing. In NaCl, the number of Fe per particle (volume) increases linearly with time while it is non-linear in $NaNO_3$. The open symbols and dotted line are for Fh aged in 0.01 M $NaNO_3$ at pH 7 in the absence of organic pH buffers, derived by interpolation of the data collected at pH 6.0 and pH 8.2 (Fig. 6).

for the soils a good correlation is found between the reactive oxide surface area and the organic matter content.[75]

As oxyanions may also interfere in the formation of Fh,[44] primary particles may remain small if these anions adsorb.[2] For instance, the adsorption of Si reduces the coherent length of scattering of Fh.[76] This explains the small size (2 nm) of siliceous Fh particles produced in drinking water facilities at aeration of groundwater with Fe(II).[27] Interference of oxyanions may also explain the small size of 2LFh (pH = 8) prepared in the presence of $As(OH)_3$.[60] The characterization with SAXS suggested a size near 2 × (0.8 + 0.2) = ~2 nm.[60] Such particles will have a surface area of ~850 m^2 g^{-1}. According to our model (Fig. 6), this would require ageing for ~0.5 hours while the particles were aged for 24 h. The difference may be due to the adsorption of $As(OH)_3$, suppressing the rate of ageing.

In literature,[51] Fh has been prepared and aged in the presence of Cl as major anion. The measured growth is very different from the growth observed in systems with NO_3 as major anion, as shown in Fig. 9 (squared colored symbols). Initially, the particles have nearly the same size in both systems. Shortly later, the time dependency of growth becomes very different. In $NaNO_3$, the rate of growth on a volume basis decreases continuously, while in NaCl the volume or number of Fe per particle (n_{Fe}) increases linearly with time.[2] This linearity is typical for a diffusion-controlled growth in systems with little super saturation, as derived by Lifshitz and Slyozov,[72] resulting in $\Delta V \propto t$ or $n_{Fe} \propto t$.

The data in Fig. 9 illustrate that the reaction pathways followed in NaCl and $NaNO_3$ are very different. In Cl systems, akaganéite (β-FeOOH·xHCl) may form as found by X-ray diffraction[77] and with HRTEM.[78] This mineral has internal sites occupied with Cl ions, giving rise to a Cl/Fe ratio of x ~ 0.15–0.19.[79,80] One may expect that such internal sites are still relatively unimportant in the initial particles from which akaganéite is formed because initially, most Fe is part of the surface and little is part of the bulk.

Conclusions

Fh is thermodynamically unstable and will ultimately transform into a more stable Fe (hydr)oxide. When initially formed, the particles are ultra-small and subject to Oswald ripening in which the smallest particles dissolve and the larger ones grow, resulting in a decrease of the reactive surface area. In the present study this pH, temperature, and time-dependent process has been probed using PO_4. We show how the time-dependent change of the surface area can be translated into the rate of growth per unit surface area (μmol Fe m^{-2} h^{-1}). In all calculations, we have accounted for the size dependency of molar mass and mass density that is the result of a variable contribution of coordinated surface water (n) in excess to the bulk composition ($FeO_{1.4}(OH)_{0.2}{\cdot}nH_2O$).

The rate of growth R is highly time-dependent and decreases by nearly three orders of magnitude at ageing from a few minutes to one week. It varies between R ~ 0.01–10 μmol m^{-2} h^{-1}. These rates can be considered as low because particle growth of Fh by a monolayer of Fe polyhedra requires 15–20 μmol m^2, *i.e.* hours or days are needed to grow a single monolayer at room temperature. Additionally, we showed that the rate of growth of Fh is too low to be limited by a diffusion flux across the solid–solution interface.

Our data only refer to primary particles (d = 1.7–2.9 nm) for which we show that the rate of growth is related to the

solubility of Fh. The data analysis reveals that the rate of growth is proportional to the square of the super saturation of the solution, expressed in the ratio of the solubility product of the actual particle (Q_{so}) and the virtual bulk (K_{so}). In our analysis, the size dependency of the solubility and super saturation is calculated using the surface Gibbs free energy of Fh (γ = 0.186 J m^{-2}) that is implemented in the Ostwald–Freundlich equation accounting for the difference in surface area of the critical and mean particle (ϕ = 3/2). The squared proportionality of the super saturation in the rate law can be interpreted as a rate limitation by a chemical reaction with dual attachment of Fe to a single site of growth (S + 2 Fe → SFe_2). The time dependency of the change of the diameter is close to $\Delta d \propto t^{1/4}$ for model and data.

The rate constant for the process of growth is pH dependent. The presence of organic pH buffers reduces the rate constant for Ostwald ripening at low pH by a factor 10 or more, but its effect disappears at high pH, which is explained by the variable interference of the organic molecules in the Fe attachment. Interference will be enhanced if Fh is covered by natural organic matter and consequently, organic matter contributes to the kinetic stability of Fh in soils.

Application of our dynamic model for particle growth discloses the initial size of non-aged Fh particles of $d \sim 1.68$ nm and the corresponding specific surface area of $A \sim 1100$ m^2 g^{-1}. These particles formed at room temperature contain on average ~45 Fe. Dynamic modeling further shows that the growth of the primary particles by Ostwald ripening is usually limited to a size of ~3.5–4 nm ($A \sim$ 350–500 m^2 g^{-1}). Additional growth will be by (oriented) particle attachment at the onset of the formation of crystal faces. This is typically observed at ageing in high temperature systems, particularly at high pH.

If 6LFh is produced with the classical method of forced hydrolysis at 75 °C, the initial particles are significantly larger (~5.5 nm). According to our model, Ostwald ripening becomes little because these particles have a relatively low solubility.

Combining various data for growth of primary Fh particles at pH = 6, collected with TEM and PO_4 probing, reveals an activation energy of E_a = 68 ± 4 kJ mol^{-1} for the growth by Ostwald ripening, which is lower than that for growth by oriented attachment.

The reaction pathway of Ostwald ripening in NaCl is very different from that in $NaNO_3$. In NaCl, the particle volume increases linearly with time while in $NaNO_3$, it is clearly nonlinear. In NaCl, akaganéite may start to form according to evidence obtained by X-ray diffraction.

Conflicts of interest

There are no conflicts to declare.

Acknowledgements

We grateful acknowledge the modelling contributions of Imtiaz Mia. Part of this project has been funded by a grant provided of the University of Costa Rica (UCR) and by Nano-NextNL (FES 5120756-02), both being gratefully acknowledged.

References

1 C. Tiberg, C. Sjostedt, I. Persson and J. P. Gustafsson, *Geochim. Cosmochim. Acta*, 2013, **120**, 140–157.
2 T. Hiemstra and W. Zhao, *Environ. Sci.: Nano*, 2016, **3**, 1265–1279.
3 L. Tian, Z. Q. Shi, Y. Lu, A. C. Dohnalkova, Z. Lin and Z. Dang, *Environ. Sci. Technol.*, 2017, **51**, 10605–10614.
4 S. Meng, H. L. Wang, H. Liu, C. H. Yang, Y. Wei and D. L. Hou, *Appl. Geochem.*, 2014, **45**, 114–119.
5 J. Liu, R. L. Zhu, T. Y. Xu, Y. Xu, F. Ge, Y. F. Xi, J. X. Zhu and H. P. He, *Chemosphere*, 2016, **144**, 1148–1155.
6 G. Pieczara and G. Rzepa, *Environ. Eng. Manage. J.*, 2016, **15**, 2095–2107.
7 D. A. Dzombak and F. M. M. Morel, *Surface complexation modeling: Hydrous Ferric Oxide*, John Wiley & Sons, New York, 1990, p. 393.
8 H. Fu, Y. Yang, R. Zhu, J. Liu, M. Usman, Q. Chen and H. He, *J. Colloid Interface Sci.*, 2018, **530**, 704–713.
9 T. D. Sowers, J. W. Stuckey and D. L. Sparks, *Geochem. Trans.*, 2018, **19**, 11.
10 L. Tian, Y. Z. Liang, Y. Lu, L. F. Peng, P. X. Wu and Z. Q. Shi, *Soil Sci. Soc. Am. J.*, 2018, **82**, 96–105.
11 A.-C. Senn, R. Kaegi, S. J. Hug, J. G. Hering, S. Mangold and A. Voegelin, *Geochim. Cosmochim. Acta*, 2017, **202**, 341–360.
12 C. P. Johnston and M. Chrysochoou, *Environ. Sci. Technol.*, 2016, **50**, 3589–3596.
13 A. Rossberg, K. U. Ulrich, S. Weiss, S. Tsushima, T. Hiemstra and A. C. Scheinost, *Environ. Sci. Technol.*, 2009, **43**, 1400–1406.
14 M. A. Larsson, I. Persson, C. Sjostedt and J. P. Gustafsson, *Environ. Chem.*, 2017, **14**, 141–150.
15 P. C. M. Francisco, T. Sato, T. Otake, T. Kasama, S. Suzuki, H. Shiwaku and T. Yaita, *Environ. Sci. Technol.*, 2018, **52**, 4817–4826.
16 X. Wang, J. D. Kubicki, J.-F. Boily, G. A. Waychunas, Y. Hu, X. Feng and M. Zhu, *ACS Earth Space Chem.*, 2018, **2**, 125–134.
17 P. J. Swedlund, H. Holtkamp, Y. Song and C. J. Daughney, *Environ. Sci. Technol.*, 2014, **48**, 2759–2765.
18 S. Zhang, P. N. Williams, C.-Y. Zhou, L. Q. Ma and J. Luo, *Chemosphere*, 2017, **184**, 812–819.
19 X. M. Wang, Y. F. Hu, Y. D. Tang, P. Yang, X. H. Feng, W. Q. Xu and M. Q. Zhu, *Environ. Sci.: Nano*, 2017, **4**, 2193–2204.
20 W. Stumm, C. P. Huang and S. R. Jenkins, *Croat. Chem. Acta*, 1970, **42**, 223–245.
21 J. A. Davis, R. James and J. O. Leckie, *J. Colloid Interface Sci.*, 1978, **63**, 480–499.
22 M. Abbas, B. P. Rao, S. M. Naga, M. Takahashi and C. Kim, *Ceram. Int.*, 2013, **39**, 7605–7611.
23 D. E. Yates, S. Levine and T. W. Healy, *J. Chem. Soc., Faraday Trans. 1*, 1974, **70**, 1807–1818.
24 T. Hiemstra and W. H. Van Riemsdijk, *J. Colloid Interface Sci.*, 1996, **179**, 488–508.

25 U. Schwertmann and R. M. Cornell, *Iron Oxides in the Laboratory*, VCH Publishers, 1991, p. 137.
26 N. Bompoti, M. Chrysochoou and M. Machesky, *Chem. Geol.*, 2017, **464**, 34–45.
27 T. Hiemstra, *Geochim. Cosmochim. Acta*, 2018, **238**, 453–476.
28 R. M. Cornell and U. Schwertmann, *The iron oxides: structures, properties, reactions, occurrence and uses*, VCH, Weinheim, 1996.
29 T. Hiemstra, *Geochim. Cosmochim. Acta*, 2015, **158**, 179–198.
30 W. Ostwald, *Z. Phys. Chem.*, 1897, **22**, 289–330.
31 D. J. Burleson and R. L. Penn, *Langmuir*, 2006, **22**, 402–409.
32 D. Li, M. H. Nielsen, J. R. I. Lee, C. Frandsen, J. F. Banfield and J. J. De Yoreo, *Science*, 2012, **336**, 1014–1018.
33 T. Hiemstra, *Environ. Sci.: Nano*, 2018, **5**, 752–764.
34 F. Huang, H. Z. Zhang and J. F. Banfield, *Nano Lett.*, 2003, **3**, 373–378.
35 P. J. Murphy, A. M. Posner and J. P. Quirk, *J. Colloid Interface Sci.*, 1976, **56**, 270–283.
36 N. D. Burrows, C. R. H. Hale and R. L. Penn, *Cryst. Growth Des.*, 2013, **13**, 3396–3403.
37 D. D. Boland, R. N. Collins, C. J. Miller, C. J. Glover and T. D. Waite, *Environ. Sci. Technol.*, 2014, **48**, 5477–5485.
38 Z. Jiang, Q. Liu, A. P. Roberts, V. Barrón, J. Torrent and Q. Zhang, *Geology*, 2018, **46**, 987–990.
39 L. Cao, Z.-X. Jiang, Y.-H. Du, X.-M. Yin, S.-B. Xi, W. Wen, A. P. Roberts, A. T. S. Wee, Y.-M. Xiong, Q.-S. Liu and X.-Y. Gao, *Environ. Sci. Technol.*, 2017, **51**, 2643–2651.
40 F. M. Michel, V. Barron, J. Torrent, M. P. Morales, C. J. Serna, J. F. Boily, Q. S. Liu, A. Ambrosini, A. C. Cismasu and G. E. Brown, *Proc. Natl. Acad. Sci. U. S. A.*, 2010, **107**, 2787–2792.
41 S. Mitsunobu, C. Muramatsu, K. Watanabe and M. Sakata, *Environ. Sci. Technol.*, 2013, **47**, 9660–9667.
42 E. E. Roden and J. M. Zachara, *Environ. Sci. Technol.*, 1996, **30**, 1618–1628.
43 U. Schwertmann, H. Stanjek and H. H. Becher, *Clay Miner.*, 2004, **39**, 433–438.
44 N. Galvez, V. Barron and J. Torrent, *Clays Clay Miner.*, 1999, **47**, 304–311.
45 R. Raiswell, H. P. Vu, L. Brinza and L. G. Benning, *Chem. Geol.*, 2010, **278**, 70–79.
46 R. M. Bolanz, U. Blass, S. Ackermann, V. Ciobotaa, P. Rosch, N. Tarcea, J. Popp and J. Majzlan, *Clays Clay Miner.*, 2013, **61**, 11–25.
47 S. Das, M. J. Hendry and J. Essilfie-Dughan, *Environ. Sci. Technol.*, 2011, **45**, 268–275.
48 J. S. Weatherill, K. Morris, P. Bots, T. M. Stawski, A. Janssen, L. Abrahamsen, R. Blackham and S. Shaw, *Environ. Sci. Technol.*, 2016, **50**, 9333–9342.
49 R. N. Collins, K. M. Rosso, A. L. Rose, C. J. Glover and T. D. Waite, *Geochim. Cosmochim. Acta*, 2016, **177**, 150–169.
50 M. Q. Zhu, C. Frandsen, A. F. Wallace, B. Legg, S. Khalid, H. Zhang, S. Morup, J. F. Banfield and G. A. Waychunas, *Geochim. Cosmochim. Acta*, 2016, **172**, 247–264.
51 Y. P. Mao, A. N. Pham, Y. J. Xin and T. D. Waite, *Sep. Purif. Technol.*, 2012, **91**, 38–45.
52 J. Antelo, F. Arce and S. Fiol, *Chem. Geol.*, 2015, **410**, 53–62.
53 X. M. Wang, F. Liu, W. F. Tan, W. Li, X. H. Feng and D. L. Sparks, *Soil Sci.*, 2013, **178**, 1–11.
54 E. B. Cerkez, N. Bhandari, R. J. Reeder and D. R. Strongin, *Environ. Sci. Technol.*, 2015, **49**, 2858–2866.
55 J. Antelo, S. Fiol, C. Perez, S. Marino, F. Arce, D. Gondar and R. Lopez, *J. Colloid Interface Sci.*, 2010, **347**, 112–119.
56 H. J. Van den Hul and J. Lyklema, *J. Am. Chem. Soc.*, 1968, **90**, 3010–3015.
57 Y. Guyodo, S. K. Banerjee, R. L. Penn, D. Burleson, T. S. Berquo, T. Seda and P. Solheid, *Phys. Earth Planet. Inter.*, 2006, **154**, 222–233.
58 N. D. Burrows, C. R. H. Hale and R. L. Penn, *Cryst. Growth Des.*, 2012, **12**, 4787–4797.
59 L. Gentile, T. Wang, A. Tunlid, U. Olsson and P. Persson, *J. Phys. Chem. A*, 2018, **122**, 7730–7738.
60 H. Guénet, M. Davranche, D. Vantelon, J. Gigault, S. Prévost, O. Taché, S. Jaksch, M. Pédrot, V. Dorcet, A. Boutier and J. Jestin, *Environ. Sci.: Nano*, 2017, **4**, 938–954.
61 R. L. Penn, J. J. Erbs and D. M. Gulliver, *J. Cryst. Growth*, 2006, **293**, 1–4.
62 J. A. Davis and J. O. Leckie, *J. Colloid Interface Sci.*, 1978, **67**, 90–107.
63 T. Hiemstra and W. H. Van Riemsdijk, *Geochim. Cosmochim. Acta*, 2009, **73**, 4423–4436.
64 T. Hiemstra, *Geochim. Cosmochim. Acta*, 2013, **10**, 316–325.
65 N. Pinney, J. D. Kubicki, D. S. Middlemiss, C. P. Grey and D. Morgan, *Chem. Mater.*, 2009, **21**, 5727–5742.
66 J. Majzlan, A. Navrotsky and U. Schwertmann, *Geochim. Cosmochim. Acta*, 2004, **68**, 1049–1059.
67 C. L. Snow, K. I. Lilova, A. V. Radha, Q. Shi, S. Smith, A. Navrotsky, J. Boerio-Goates and B. F. Woodfield, *J. Chem. Thermodyn.*, 2013, **58**, 307–314.
68 A. Navrotsky, L. Mazeina and J. Majzlan, *Science*, 2008, **319**, 1635–1638.
69 B. Molleman and T. Hiemstra, *Phys. Chem. Chem. Phys.*, 2018, **20**, 20575–20587.
70 R. H. Byrne and Y. R. Luo, *Geochim. Cosmochim. Acta*, 2000, **64**, 1873–1877.
71 F. Y. Li, L. Koopal and W. F. Tan, *Sci. Rep.*, 2018, **8**, 13.
72 I. M. Lifshitz and V. V. Slyozov, *J. Phys. Chem. Solids*, 1961, **19**, 35–50.
73 C. Wagner, *Z. Elektrochem.*, 1961, **65**, 581–591.
74 M. V. Speight, *Acta Metall.*, 1968, **16**, 133–135.
75 T. Hiemstra, J. Antelo, R. Rahnemaie and W. H. van Riemsdijk, *Geochim. Cosmochim. Acta*, 2010, **74**, 41–58.
76 A. C. Cismasu, F. M. Michel, A. P. Tcaciuc, T. Tyliszczak and G. E. Brown, *C. R. Geosci.*, 2011, **343**, 210–218.
77 G. Biedermann and J. T. Chow, *Acta Chem. Scand.*, 1966, **20**, 1376–1388.
78 B. A. Legg, M. Q. Zhu, H. Z. Zhang, G. Waychunas, B. Gilbert and J. F. Banfield, *Cryst. Growth Des.*, 2016, **16**, 5726–5737.
79 P. A. Kozin and J.-F. Boily, *J. Phys. Chem. C*, 2013, **117**, 6409–6419.
80 M. Kersten, S. Karabacheva, N. Vlasova, R. Branscheid, K. Schurk and H. Stanjek, *Colloids Surf., A*, 2014, **448**, 73–80.